Journal of Chromatography A, 1218 (2011) 1677–1690

Contents lists available at ScienceDirect

Journal of Chromatography A

journal homepage: www.elsevier.com/locate/chroma

A validated model for the simulation of protein purification through affinity membrane chromatography☆

Simone Dimartino, Cristiana Boi, Giulio C. Sarti*

Dipartimento di Ingegneria Chimica, Mineraria e delle Tecnologie Ambientali, DICMA, Università di Bologna, via Terracini 28, 40131 Bologna, Italy

ARTICLE INFO

Article history:
Received 28 October 2010
Received in revised form
18 November 2010
Accepted 23 November 2010
Available online 27 November 2010

Keywords:
Membrane chromatography
Affinity chromatography
Protein purification
Mathematical model
Membrane column model

ABSTRACT

A mathematical model is proposed for the description of protein purification through membrane affinity chromatography. The model describes all the three stages of the chromatographic cycle and takes into account convection, axial dispersion and binding reaction kinetics in the porous membrane matrix, while boundary layer mass transfer resistance is shown to be negligible. All the model parameters have a precise physical meaning which enables their evaluation through separate experimental measurements, independent of the chromatographic cycle. Model testing and validation has been performed with experimental chromatographic cycles carried out with pure IgG solutions as well as with complex mixtures containing IgG_1, using new affinity membranes. The comparison between model calculations and experimental data showed good agreement for all stages of the affinity cycle. In particular, for loading and washing steps binding kinetics was found so fast that adsorption equilibrium was sufficient to describe the observed behavior; as a result, the model simulations are entirely predictive for the adsorption and washing phases. On the contrary, in the elution step the reaction rate is comparable to that of the other simultaneous transport phenomena. The model is able to predict the performance of chromatographic purification of IgG from complex mixtures simply on the basis of the parameter values obtained from pure IgG solutions.

1. Introduction

Since its first introduction in 1953 by Lerman [1], the use of affinity chromatography by the biotechnology industry for the manufacture of high purity products is continuously experiencing a fast growth [2–4]. Affinity chromatography techniques exploit the bio-specific interactions between a target molecule and a proper ligand immobilized on a porous matrix. Generally, an affinity cycle consists of at least three subsequent stages: loading, washing and elution. In the first step the sample is loaded to the affinity column until the desired column saturation is reached; complete saturation is eventually attained when all the affinity sites are occupied by the target protein. After loading, the column is thoroughly washed with a suitable buffer in order to remove non-specifically adsorbed species. Finally, in the last step the buffer is conveniently changed in order to elute and recover the target molecule. A regeneration stage is periodically required to restore the initial behavior of the stationary phase.

Traditionally, affinity chromatography is performed in columns packed with porous beads; however, slow diffusive mass transport, high pressure drops and bead compressibility represent some of the drawbacks associated with such supports. In the last decades, stationary phases allowing access to the active affinity sites only through convective transport, such as microporous membranes, are receiving increasing attention since they can actually overcome the limitations listed above. Indeed, in comparison to affinity beads, membrane affinity chromatography can operate at higher flow rates and lower operative pressures; this translates into a faster and more cost-effective purification process [5–9].

The analysis of mass transfer and kinetic phenomena involved in membrane affinity chromatography may be useful to understand the overall separation mechanism and is required for process optimization and scale up purposes. To simulate the chromatographic process different mathematical models have been proposed, characterized by different complexity levels in the description of the relevant mass transfer phenomena [10,11]. In order to accurately take into account all mass transfer contributions that can possibly play a role, a general rate (GR) model has also been developed [12]. The solution of the GR model requires considerable computational time and/or advanced numerical algorithms, as well as the need of a number of fitting parameters or empirical correlations to estimate physical quantities that are *a priori* unknown [13–15].

The general rate model is often rearranged in simplified forms in which different mass transfer processes are expressed as a single term, as the lumped kinetic model or the lumped pore model considered by Guiochon et al. [16,17]. Of course, lumped models are

☆ Presented at the 30th International Symposium on Proteins, Peptides and Polynucleotides (ISPPP), Bologna, Italy, 5–8 September 2010.

* Corresponding author. Tel.: +39 051 2090251; fax: +39 051 2090247.
E-mail address: giulio.sarti@unibo.it (G.C. Sarti).

0021-9673/$ – see front matter © 2010 Elsevier B.V. All rights reserved.
doi:10.1016/j.chroma.2010.11.056

much simpler for computational purposes, however the physical meaning of some of their parameters may disappear completely, as it happens in the case of the unacceptable flow rate dependence of the kinetic rate constant that has been reported by several authors [18–22], which seriously questions the applicability of the model for process optimization and scale up purposes.

Other empirical approaches, as multivariable methods and principal component analysis, evaluate the intervening parameters through a complex and elaborated form of interpolation of available data [23]. However, their use outside the range of experimental data considered in the instruction stage is not allowed, thus preventing one of the main uses of the model as scaling up the process.

In order to develop an effective simulation tool, reliable for prediction, optimization and scale up purposes, the model must be physically based, as simple as possible and at the same time able to describe all the relevant physical phenomena which play a role. In that case, all the model parameters have a precise physical meaning and their value can generally be obtained through separate independent experiments. To that aim, the analysis starts from a detailed inventory of the relevant mechanisms which affect the separation process and its kinetics; proper simplifications in the equations of the general rate model can then be introduced on the basis of order of magnitude estimations applied to the stationary phase under investigation. Following this approach, the resulting model may also gain computational simplification without any loss of reliability for predicting purposes and robustness.

In the present work, the latter approach is used to derive a suitable and practical model for the description of protein purification by means of membrane affinity chromatography. The proposed model has been formulated to describe all the three stages of membrane affinity chromatography process. Indeed, many simulation studies are available for the description of the breakthrough profile obtained in the adsorption stage [24–28] while, in contrast, modeling analysis for the washing and elution stages is frequently disregarded.

Finally, the proposed model is also used to simulate and predict complete chromatographic cycles experimentally studied for the purification of human IgG from a complex feedstock using B14-TRZ-Epoxy2 affinity membranes under various different operating conditions. The influence of flow rate and feed protein concentration on breakthrough and washing profiles as well as on the elution peaks have been analyzed and discussed in detail.

2. Theoretical

The general model suitable for the entire chromatographic cycle must account for the relevant kinetic and transport phenomena occurring inside the membrane column in all process stages; it must describe also the effects of fluid dynamics in the plant units, beyond the affinity module, that are located between the feed reservoir and the detector cell analyzing the effluent solution concentration. The membrane column model is based on the species mass balance over the membrane stack, including the kinetic equations that describe the binding/unbinding of the protein onto/from the immobilized ligand. The system dispersion model describes the fluid flow non-idealities occurring in all the volumes of the chromatographic system external to the membrane column.

2.1. System dispersion model

The concentration of the solutes is monitored in the feed tank and in the detector cell placed after the affinity column. Therefore, the experimental system is composed of the membrane column and of a series of ancillary external elements including pumps, valves, on-line filters, tubing, fittings, column distributor and collector, etc. The overall volume of those elements is often of the same order of magnitude of the membrane column volume, at least at laboratory or pilot plant scale [29]. Thus the response of the chromatographic system is also affected by the flow non-idealities occurring in all the external elements, resulting in deviations from pure plug flow behavior, globally indicated as system dispersion effects [30]. By neglecting system dispersion the response of the chromatographic system is not appropriately described and the simulation results for the affinity unit cannot be properly compared in a quantitative manner to the experimental results; in particular, neglecting external system dispersion may result into an exceedingly large axial dispersivity coefficient of the porous medium [31], as well as in an incorrect estimation of equilibrium binding data [32].

The main flow non-idealities are due to mixing volumes and dead volumes, therefore the simplest model that can simulate the resulting behavior couples a continuous stirred tank reactor (CSTR) and a plug flow reactor (PFR) in series, whose volumes are V_{CSTR} and V_{PFR}, respectively; the total system volume, V_{SYS}, external to the chromatography bed can thus be divided into the following contributions:

$$V_{SYS} = V_{PFR} + V_{CSTR} \tag{1}$$

Since in common chromatographic systems the external volumes are mainly located upstream the affinity column, it is here considered that system dispersion effects are globally condensed before the membrane stack. Hence, the exit stream from the system dispersion model, represents the inlet for the membrane column model.

The species balance equations of the constant volume CSTR and PFR are expressed as usual:

$$\frac{dc_{i,out}^{CSTR}}{dt} = \frac{F}{V_{CSTR}}(c_{i,in}^{CSTR} - c_{i,out}^{CSTR}) \tag{2}$$

$$c_{i,out}^{PFR} = \begin{cases} 0 & \text{for } t < t_d \\ c_{i,in}^{PFR} & \text{for } t \geq t_d \end{cases} \tag{3}$$

where F is the volumetric flow rate, c_i is the solute concentration of the species i, subscripts *in* and *out* label inlet and outlet values, respectively, and $t_d = V_{PFR}/F$ is the delay time associated to the PFR. It is worth noticing that the position of the CSTR with respect to the PFR has no influence on the system dispersion model results, since a PFR causes a pure delay in the output response. In this work we consider the configuration of a CSTR followed by a PFR and thus:

$$c_{i,out}^{CSTR} = c_{i,in}^{PFR} \tag{4}$$

The initial condition for the CSTR, as well as its inlet concentration, $c_{i,in}^{CSTR}$, depend on the chromatographic process stage. At the beginning of the loading step, i.e. at time t_0^{ads}, there is no target protein inside the chromatographic system, while the inlet protein concentration corresponds to the feed protein concentration, $c_{i,0}$, thus:

$$c_{i,out}^{CSTR} = 0 \quad \text{for } t = t_0^{ads} \tag{5}$$

$$c_{i,in}^{CSTR} = c_{i,0} \quad \text{for } t_0^{ads} \leq t < t_0^{was} \tag{6}$$

After loading, the washing step starts at time t_0^{was}, at which the protein concentration in the system corresponds to the feed protein concentration whenever the adsorption step lasts for a time span long enough with respect to the residence time in the system volume. Also, during the washing step no protein is fed into the system, thus:

$$c_{i,out}^{CSTR} = c_{i,0} \quad \text{for } t = t_0^{was} \tag{7}$$

$$c_{i,in}^{CSTR} = 0 \quad \text{for } t_0^{was} \leq t < t_0^{elu} \tag{8}$$

It is worth noticing that, in view of the well known time evolution of concentration in a CSTR, (see e.g. Eq. (13) below), Eq. (7) is strictly valid only if the feed volume in the adsorption step is larger than about $3 \cdot V_{CSTR}$, that is the volume needed to attain the 95% of the feed concentration inside the CSTR, positioned before the PFR in the system dispersion model. However, this condition is almost always true for laboratory scale and pilot plant set up. Alternatively, the initial concentration for the washing step is equal to the final value resulting from the loading stage.

After the washing step elution starts at time t_0^{elu} and the inlet protein concentration remains equal to zero. Consequently, the protein concentration exiting the system dispersion model is zero throughout the entire elution stage. Analogously to what pointed out for Eq. (7), this conclusion is strictly valid only if the washing volume applied is larger than about $3 \cdot V_{CSTR}$, which is a condition usually satisfied in careful washing steps.

System dispersion affects also the eluent species that are introduced during elution, whose concentration, c_e, is given by a mass balance similar to that used for the system dispersion model in the adsorption step:

$$\frac{dc_{e,out}^{CSTR}}{dt} = \frac{F}{V_{CSTR}}(c_{e,in}^{CSTR} - c_{e,out}^{CSTR}) \tag{9}$$

$$c_{e,out}^{PFR} = \begin{cases} 0 & \text{for } t < t_d + t_0^{elu} \\ c_{e,in}^{PFR} & \text{for } t \geq t_d + t_0^{elu} \end{cases} \tag{10}$$

$$c_{e,out}^{CSTR} = 0 \quad \text{for } t = t_0^{elu} \tag{11}$$

$$c_{e,in}^{CSTR} = c_{e,0} \quad \text{for } t > t_0^{elu} \tag{12}$$

Under the initial and boundary conditions considered, the system dispersion model leads to the following analytical solutions:

$$c_{i,SD} = \begin{cases} 0 & \text{when } t_0^{ads} \leq t < t_0^{ads} + t_d \\ c_{i,0}\left[1 - \exp\left(-\frac{F}{V_{CSTR}}(t - (t_d + t_0^{ads}))\right)\right] & \text{when } t_d + t_0^{ads} \leq t < t_0^{was} \\ c_{i,0} & \text{when } t_0^{was} \leq t < t_0^{was} + t_d \\ c_{i,0}\exp\left(-\frac{F}{V_{CSTR}}(t - (t_d + t_0^{was}))\right) & \text{when } t_d + t_0^{was} \leq t < t_0^{elu} \\ 0 & \text{when } t_0^{elu} \leq t \end{cases} \tag{13}$$

$$c_{e,SD} = \begin{cases} 0 & \text{when } t_0^{ads} \leq t < t_0^{elu} + t_d \\ c_{e,0}\left[1 - \exp\left(-\frac{F}{V_{CSTR}}(t - (t_d + t_0^{elu}))\right)\right] & \text{when } t_d + t_0^{elu} \leq t \end{cases} \tag{14}$$

where $c_{i,SD}$ and $c_{e,SD}$ are the concentrations of protein and eluent species, respectively, actually entering the membrane column due to the system dispersion response.

2.2. Membrane column model

The membrane column is schematically considered as an ideal porous medium of total length L, with uniform porosity ε, and uniform membrane capacity in the solid phase q_m. The pore diameter is assumed to be equal to the membrane mean pore diameter, d_p, since it has been demonstrated that the effects of a pore size distribution can be neglected when the membrane stack is sufficiently thick [24,25]. The interstitial flow velocity, v, is constant and uniform over the column as a result of an effective flow distribution and collection at the column inlet and outlet. Of course, if the flow distribution in the radial direction is poor or not effective one needs to use the local interstitial velocity at any point of the membrane column, which can be determined experimentally from separate tests. In our case, model validation is performed using experimental data for which uniform velocity was actually detected and there is no need to formally use an interstitial velocity which varies in the radial direction [33,34]. This allows also to consider one dimensional problem only, without the need to include radial variations of the concentration values of all the species.

2.2.1. Relevant transport mechanisms

From a general standpoint, mass transport of a solute in the fluid phase inside a porous medium may occur by axial convection, axial dispersion and boundary layer mass transfer; other transport mechanisms, such as axial diffusion or surface diffusion, are also formally present but it was already shown that they are not relevant in the case of microporous membranes and, based on that, they are disregarded hereafter [25].

With the aim to simplify as far as possible the governing equations and to consider only the main transport phenomena involved in the separation process, the characteristic time scales associated to the relevant mechanisms are here examined. It is thus shown that the relevant transport phenomena in membrane chromatographic columns are axial convection and longitudinal dispersion, whereas boundary layer mass transfer can be completely neglected. Such a result is important since different interpretations have been given about the main transport mechanisms relevant in membrane chromatography; indeed, different authors neglect the contribution of boundary layer mass transfer [29,35,36] while several others do not consider axial dispersion as a significant transport phenomenon [24,27,30,37].

The characteristic time scales for axial convection, τ_C, longitudinal dispersion, τ_L, and film boundary layer mass transfer between bulk fluid and pore surface, τ_F, can be defined as [38]:

$$\tau_C = \frac{L}{v} \tag{15}$$

$$\tau_L = \frac{L^2}{D_L} \tag{16}$$

$$\tau_F = \frac{\delta}{k_F} \tag{17}$$

where δ is the thickness of the diffusive layer, k_F is the boundary layer mass transfer coefficient between liquid and pore surface, L is the membrane stack thickness and D_L is the axial dispersion coefficient.

An estimation of the boundary layer mass transfer coefficient can be obtained by applying the well known film theory [38]:

$$k_F \cong \frac{D_m}{\delta} \tag{18}$$

where D_m is the molecular diffusion coefficient. By considering that half of the mean pore radius, namely $d_p/4$, is a reasonable overestimation for the thickness of the diffusive layer, the boundary layer mass transfer time scale, τ_F, can be safely estimated as:

$$\tau_F \cong \left(\frac{d_p}{4}\right)^2 \frac{1}{D_m} \tag{19}$$

Table 1
Typical values of the variables used in membrane chromatographic processes.

Variable	Value	Reference
d_p (cm)	10^{-4}	[39–44]
v (cm/s)	10^{-4}–10^{-2}	[39–43]
L (cm)	10^{-2}–1	[40–44]
D_L (cm^2/s)	$<10^{-3}$	[19,26,39]
D_m (cm^2/s)	10^{-7}	[45]

The values of the parameters used for the evaluation of τ_C, τ_L and τ_F are reported in Table 1, as obtained from different literature sources which consider the purification of several proteins, ranging from lysozyme to immunoglobulin G, using different chromatographic modes and membrane modules that differ in scale and configuration. The resulting characteristic time scales are:

$$\tau_C \cong 10^0\text{–}10^4\ \text{s}$$

$$\tau_L > 10^{-1}\text{–}10^3\ \text{s}$$

$$\tau_F \cong 10^{-2}\ \text{s}$$

It is apparent that the characteristic time for boundary layer mass transfer is at least one order of magnitude lower than the time scale for axial dispersion and two orders of magnitude lower than the time scale for convection. More precisely, the value reported of $\tau_F \cong 10^{-2}$ s represents an upper limit which in practical applications will never be reached, since the boundary layer mass transfer coefficient has been underestimated.

Thus, the boundary layer mass transfer is a fast transport phenomenon with respect to the other mechanisms involved in membrane chromatographic separations, and its contribution to the overall rate can be neglected in the mathematical formulation. On the contrary, axial convection and longitudinal dispersion are the most relevant transport phenomena and must be taken into account.

This conclusion is supported also by the experimental evidence reported by Gerstner et al. [46] who found that the height equivalent to a theoretical plate (HETP) of a membrane column is insensitive to flow rate in experiments performed with two different membrane packings, using human transferrin and cytochrome C as tracers.

A further evidence is offered by the experimental studies performed independently on membrane adsorbers by Frey et al. [47] and by Shiosaki et al. [48], who also concluded that axial dispersion is the dominant transport mechanism in membrane chromatographic media.

Based on the above conclusions and under the assumptions of uniform porosity and uniform interstitial velocity, the species mass balance equation which properly describes the membrane column behavior becomes:

$$\varepsilon\frac{\partial c_i}{\partial t} + \varepsilon v\frac{\partial c_i}{\partial z} = \varepsilon D_{L,i}\frac{\partial^2 c_i}{\partial z^2} - (1-\varepsilon)\frac{\partial q_i}{\partial t} \tag{20}$$

where z is the axial coordinate and q_i is the concentration of the adsorbed protein per unit volume of stationary phase.

Danckwerts boundary conditions for frontal analysis are used to account for axial dispersion at the front surface of the membrane, and mixing at the exit of the membrane [49]:

$$vc_i - D_{L,i}\frac{\partial c_i}{\partial z} = vc_{i,SD} \quad \text{for} \quad z = 0, \quad t > 0 \tag{21}$$

$$\frac{\partial c_i}{\partial z} = 0 \quad \text{for} \quad z = L, \quad t > 0 \tag{22}$$

It is worth noticing that the protein concentration at the inlet of the membrane stack is not equal to the protein concentration fed to the system, $c_{i,0}$, but it is rather the value $c_{i,SD}$, due to the dispersion in the system preceding the membrane column and given by the response of the external dispersion model (Eq. (13)).

Eq. (20) together with Eqs. (21) and (22) will be adopted for all the three stages of the entire affinity cycle, while the specific kinetic mechanism as well as the specific initial conditions must be adapted to the single process stage considered.

2.2.2. Adsorption step

During loading the biological solution is fed into the column and the target protein is adsorbed on the membrane active sites. Throughout this stage, the concentration in the feed tank, $c_{i,0}$, is kept constant for $t \in (t_0^{ads}, t_0^{was})$, while the actual feed reaches the inlet of the membrane column for $t \in (t_0^{ads} + t_d, t_0^{was} + t_d)$, with values given in Eq. (13).

For homogeneous adsorption in a monolayer, the Langmuir approach can be used successfully for the adsorption kinetics [50], thus during loading the mass balance in the membrane column, Eq. (20), becomes:

$$\varepsilon\frac{\partial c_i}{\partial t} + \varepsilon v\frac{\partial c_i}{\partial z} = \varepsilon D_{L,i}\frac{\partial^2 c_i}{\partial z^2} - (1-\varepsilon)k_a c_i\left[(q_m - q_i) - K_d\frac{q_i}{c_i}\right]$$

$$\text{for} \quad 0 < z < L, \quad t_0^{ads} + t_d < t < t_0^{was} + t_d \tag{23}$$

where $K_d = k_d/k_a$ is the Langmuir dissociation equilibrium constant, k_a and k_d are the kinetic constants for binding and unbinding reactions and q_m is the maximum binding capacity.

The general expression embodied by Eq. (23) can be further simplified in the case in which adsorption and desorption are much faster in comparison to convection and dispersion, so that the protein–ligand reaction can be considered instantaneously at equilibrium. Kochan et al. derived that under such conditions the breakthrough curves must be independent of feed flow rate [40]. This feature was indeed experimentally observed by several authors studying different membrane chromatographic systems [25,41,43,48], and it was also the case for the experimental system under investigation [34,51].

If equilibrium is instantly attained between the mobile and solid phases, the concentration of the target protein in solution, c_i, and on the support, q_i, are directly related to one another by the Langmuir isotherm:

$$q_i = \frac{c_i q_m}{c_i + K_d} \quad \text{for} \quad 0 \le z \le L, \quad t_0^{ads} + t_d < t < t_0^{was} + t_d \tag{24}$$

and the time rate of change of q_i is only associated to the time rate of change of the protein concentration in solution so that:

$$\frac{\partial q_i}{\partial t} = \frac{q_m K_d}{(c_i + K_d)^2}\frac{\partial c_i}{\partial t} \quad \text{for} \quad 0 \le z \le L, \quad t_0^{ads} + t_d < t < t_0^{was} + t_d \tag{25}$$

Thus, substituting this result into Eq. (20), the species balance equation becomes:

$$\frac{\partial c_i}{\partial t}\left[1 + \frac{(1-\varepsilon)}{\varepsilon}\frac{q_m K_d}{(c_i + K_d)^2}\right] + v\frac{\partial c_i}{\partial z} = D_{L,i}\frac{\partial^2 c_i}{\partial z^2}$$

$$\text{for} \quad 0 < z < L, \quad t_0^{ads} + t_d < t < t_0^{was} + t_d \tag{26}$$

The equation above represents the core of the so called equilibrium dispersive model for membrane chromatography, in which the binding reaction is at equilibrium and dispersion is non-negligible in the convective medium. The initial condition for Eq. (26) indicates that at the beginning of loading there is no protein in the column:

$$c_i = 0 \quad \text{for} \quad 0 < z < L, \quad t = t_0^{ads} + t_d \tag{27}$$

The situation described above characterizes efficient membrane chromatographic modules where the characteristic reaction time

for adsorption, $\tau_a = 1/k_a c_i$, is much shorter than all three relevant characteristic times due to convection, τ_C, axial dispersion, τ_L, and current process, τ_P, namely when the following conditions hold true:

$$(1-\varepsilon)\tau_a << \varepsilon\tau_C; \quad (1-\varepsilon)\tau_a << \varepsilon\tau_L; \quad (1-\varepsilon)\tau_a << \varepsilon\tau_P \tag{28}$$

The process time scale is the time elapsed since the onset of breakthrough. When Eqs. (28) are satisfied the species balance Eq. (20) simplifies into Eq. (26); alternatively, when the contribution of binding/unbinding kinetics is not negligible, Eq. (20) becomes Eq. (23).

For the experimental system considered in the present work, the conditions of Eqs. (28) are satisfied, as it will be verified in Section 4.2.1, allowing the use of the equilibrium dispersive model.

2.2.3. Washing step

After loading, for $t \in (t_0^{was}, t_0^{elu})$ the feed is changed into the washing solution which enters the membrane column in the time interval between $t_0^{was} + t_d$ and $t_0^{elu} + t_d$. Washing is ended when the overall concentration of contaminants or undesired species in the effluent reaches the desired value of practically zero.

One of the major advantages of affinity chromatography over other chromatographic methods is represented by the high stability of the protein–ligand interactions, which are not disrupted during the washing step [37]. Thus, the concentration of the target protein specifically adsorbed on the support remains constant during washing and the accumulation on the membrane surface is set to zero:

$$\frac{\partial q_i}{\partial t} = 0 \quad \text{for} \quad 0 \le z \le L, \quad t_0^{was} + t_d < t < t_0^{elu} + t_d \tag{29}$$

The mass transport equation during washing is represented by Eq. (20) with the condition given by Eq. (29), so that the mass balance equation for the protein in solution in the membrane column reduces simply to the following form:

$$\frac{\partial c_i}{\partial t} + v\frac{\partial c_i}{\partial z} = D_{L,i}\frac{\partial^2 c_i}{\partial z^2} \quad \text{for} \quad 0 < z < L, \quad t_0^{was} + t_d < t < t_0^{elu} + t_d \tag{30}$$

In laboratory scale experiments, it is common practice to load the column until complete saturation, that is adsorption is ended when the protein adsorbed onto the membranes is in equilibrium with the protein concentration in the feed. Under those conditions, the protein concentration in solution is equal to the feed protein concentration, and the initial condition for the washing step is:

$$c_i = c_{i,0} \quad \text{for} \quad 0 < z < L, \quad t = t_0^{was} + t_d \tag{31}$$

2.2.4. Elution step

The mass balance equation for the elution stage, taking place in the membranes for times greater than $t_0^{elu} + t_d$, is again given by Eq. (20); the time rate of change of concentration of the immobilized protein, $r_e = \partial q_i/\partial t$, needs to be defined according to the appropriate elution kinetics.

For non-selective elution, the buffer alters the local interactions of the adsorbate–ligand complex promoting its dissociation. Under these conditions the dissociation kinetics is likely irreversible, since when the interactions between the ligand and the adsorbate are disrupted the protein does not interact any longer with the affinity support. The elution peaks experimentally observed are highly dependent on flow rate (see e.g. Fig. 10) [34,51]; this observation suggests that the time scale for elution is of the same order of magnitude of the time scale for convection, and thus it is not possible to consider protein desorption during elution as an instantaneous process. Moreover, it is appropriate to consider that the dissociation of the adsorbate–ligand complexes occurs in the column only when the local eluent concentration, c_e, exceeds a critical value, $c_{e,crit}$, which makes the elution reaction effective [52]. That can be synthetically expressed by using the Heaviside step function, $u(c_e - c_{e,crit})$, as multiplying factor in the elution kinetic equation.

In this work, two different elution kinetics are considered: (i) a second order elution kinetics containing the concentrations of both the eluting agent and the adsorbed protein:

$$r_e = \frac{\partial q_i}{\partial t} = -k_{e,2} \cdot q_i c_e \cdot u(c_e - c_{e,crit}) \quad \text{for} \quad 0 \le z \le L, \quad t > t_0^{elu} + t_d \tag{32}$$

and (ii) a pseudo first order kinetic equation, where only the concentration of the adsorbed protein is explicitly present while the eluent concentration is lumped into the elution kinetic rate constant:

$$r_e = \frac{\partial q_i}{\partial t} = -k_{e,1} \cdot q_i \cdot u(c_e - c_{e,crit}) \quad \text{for} \quad 0 \le z \le L, \quad t > t_0^{elu} + t_d \tag{33}$$

After using the kinetic equations for the elution step, Eq. (32) or (33), Eq. (20) is solved with the following initial condition for the protein concentration in solution:

$$c_i = 0 \quad \text{for} \quad 0 < z < L, \quad t = t_0^{elu} + t_d \tag{34}$$

consistent with the fact that the washing step is ended when the protein concentration in the liquid phase of the column is practically zero. The initial condition for the protein concentration on the affinity support is expressed considering a uniform value in the column, $q_{0,e}$:

$$q_i = q_{0,e} \quad \text{for} \quad 0 \le z \le L, \quad t > t_0^{elu} + t_d \tag{35}$$

Finally, since the elution kinetic equations, Eqs. (32) and (33), contain the concentration of the eluent agent, c_e, its calculation at any time and axial position is also required, and therefore an additional species balance equation for the eluent is needed. In most practical cases, the non-selective eluent is a small molecule, such as an inorganic salt or a low molecular weight organic compound [53]; thus boundary layer mass transfer is faster than for proteins, and its presence, already negligible for proteins, can be disregarded *a fortiori* for the eluent. In addition, a proper eluent does not adsorb on the stationary phase, so that its mass balance in the membrane column reduces to:

$$\frac{\partial c_e}{\partial t} + v\frac{\partial c_e}{\partial z} = D_{L,e}\frac{\partial^2 c_e}{\partial z^2} \quad \text{for} \quad 0 < z < L, \quad t > t_0^{elu} + t_d \tag{36}$$

where $D_{L,e}$ is the longitudinal dispersion coefficient for the eluent species. The corresponding initial and boundary conditions are:

$$c_e = 0 \quad \text{for} \quad 0 < z < L, \quad t = t_0^{elu} + t_d \tag{37}$$

$$vc_e - D_{L,e}\frac{\partial c_e}{\partial z} = vc_{e,SD} \quad \text{for} \quad z = 0, \quad t > t_0^{elu} + t_d \tag{38}$$

$$\frac{\partial c_e}{\partial z} = 0 \quad \text{for} \quad z = L, \quad t > t_0^{elu} + t_d \tag{39}$$

where $c_{e,SD}$ is the eluent concentration entering the membrane column and is determined from the system dispersion model, Eq. (14).

2.3. Summary of the mathematical model

In order to provide a synthetic summary of the mathematical formalism discussed above, a schematical overview of the sequence of apparatuses is reported in Fig. 1, while the fundamental equations adopted for each chromatographic stage involved in the separation process are detailed in Table 2 together with their corresponding initial conditions.

Table 2
Summary of the relevant model equations.

	Time	Membrane inlet concentrations	Equations governing the concentration in the liquid solution in the membrane column
Adsorption	$t_0^{ads} < t < t_0^{ads} + t_d$	$\begin{cases} c_{i,SD} = 0 \\ c_{e,SD} = 0 \end{cases}$	
	$t_0^{ads} + t_d < t < t_0^{was}$	$\begin{cases} c_{i,SD} = c_{i,0}\left[1 - \exp\left(-\frac{F}{V_{CSTR}}(t - (t_d + t_0^{ads}))\right)\right] \\ c_{e,SD} = 0 \end{cases}$	$\begin{cases} \frac{\partial c_i}{\partial t}\left[1 + \frac{(1-\varepsilon)}{\varepsilon}\frac{q_m K_d}{(c_i + K_d)^2}\right] + v\frac{\partial c_i}{\partial z} = D_{L,i}\frac{\partial^2 c_i}{\partial z^2} \\ \text{initial condition}: \quad c_i = 0 \\ c_e = 0 \end{cases}$
Washing	$t_0^{was} < t < t_0^{was} + t_d$	$\begin{cases} c_{i,SD} = c_{i0} \\ c_{e,SD} = 0 \end{cases}$	
	$t_0^{was} + t_d < t < t_0^{elu}$	$\begin{cases} c_{i,SD} = c_{i,0}\exp\left(-\frac{F}{V_{CSTR}}(t - (t_d + t_0^{was}))\right) \\ c_{e,SD} = 0 \end{cases}$	$\begin{cases} \frac{\partial c_i}{\partial t} + v\frac{\partial c_i}{\partial z} = D_{L,i}\frac{\partial^2 c_i}{\partial z^2} \\ \text{initial condition}: \quad c_i = c_{i,0} \\ c_e = 0 \end{cases}$
Elution	$t_0^{elu} < t < t_0^{elu} + t_d$	$\begin{cases} c_{i,SD} = 0 \\ c_{e,SD} = 0 \end{cases}$	
	$t_0^{elu} + t_d < t$	$\begin{cases} c_{i,SD} = 0 \\ c_{e,SD} = c_{e,0}\left[1 - \exp\left(-\frac{F}{V_{CSTR}}(t - (t_d + t_0^{elu}))\right)\right] \end{cases}$	$\begin{cases} \frac{\partial c_i}{\partial t} + v\frac{\partial c_i}{\partial z} = D_{L,i}\frac{\partial^2 c_i}{\partial z^2} + \frac{(1-\varepsilon)}{\varepsilon}r_e \\ \frac{\partial c_e}{\partial t} + v\frac{\partial c_e}{\partial z} = D_{L,e}\frac{\partial^2 c_e}{\partial z^2} \\ \text{initial conditions}: \quad c_i = 0; \quad q_i = q_{0,e}; \quad c_e = 0 \end{cases}$

3. Determination of model parameters

One of the most important issues in model development and analysis is represented by the procedures followed to determine the numerical values of the model parameters. The main advantage of physically based mathematical models, as the one considered in the present work, resides in the fact that all the model parameters have a precise physical meaning, which generally allows for their determination through separate experimental tests independent of the process under investigation.

In the following, the procedures adopted to obtain the values of the model parameter through independent measurement are briefly presented and discussed. An important tool to that aim is represented by the conventional method of statistical moments applied to the chromatographic peaks resulting from a narrow rectangular pulse injection of the sample solution into the system [54,55]. This method is an effective approach to derive the actual volume, porosity and dispersion coefficient of the membrane medium.

The first moment, μ_1, and the second central moment, $\overline{\mu}_2$, of a chromatographic peak are expressed as follows:

$$\mu_1 = \frac{\int_0^\infty c_j(L,t)\cdot t\,dt}{\int_0^\infty c_j(L,t)\,dt} \tag{40}$$

$$\overline{\mu}_2 = \frac{\int_0^\infty c_j(L,t)\cdot (t-\mu_1)^2\,dt}{\int_0^\infty c_j(L,t)\,dt} \tag{41}$$

where $c_j(L,t)$ is the concentration of the probe species j at the exit section, at time t.

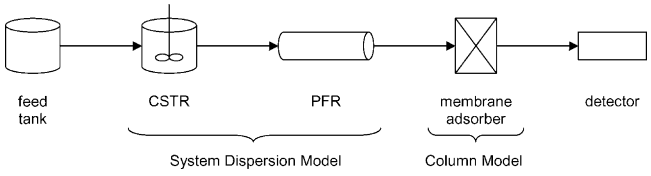

Fig. 1. Experimental set up schematization for modeling purposes.

Since for the system under investigation the external volumes are of the same order of magnitude of the membrane column volume, it is necessary to consider also their contributions to the first moment and to the second central moment, in addition to that arising from the injection of the probe. Each source of band spreading has a separate and additive contribution to the two moments [56,57], and thus the following relationships hold:

$$\mu_1^{tot} = \mu_1^{mem} + \mu_1^{inj} + \mu_1^{ext} \tag{42}$$

$$\overline{\mu}_2^{tot} = \overline{\mu}_2^{mem} + \overline{\mu}_2^{inj} + \overline{\mu}_2^{ext} \tag{43}$$

where superscripts *tot*, *mem*, *inj* and *ext* label the first moments (μ_1) and the second central moments ($\overline{\mu}_2$) of the overall plant unit, membrane column, injection pulse and external volumes, respectively. The injection terms depend only on the time duration of the pulse, t_p, according to the simple relations $\mu_1^{inj} = t_p/2$ and $\overline{\mu}_2^{inj} = {t_p}^2/12$ [58]. The external contributions are determined by performing analogous pulse experiments in the absence of the stationary phase.

For stacked membrane columns, when pulse experiments are carried out under non-adsorbing conditions, the following relationships for the two moments hold true:

$$\mu_1^{mem} = \frac{L}{v} \equiv \frac{V_{mem}}{F/\varepsilon} \tag{44}$$

$$\overline{\mu}_2^{mem} = \frac{2LD_L}{v^3} \tag{45}$$

where the right-hand side of Eq. (44) is obtained by multiplying numerator and denominator by the membrane frontal area A and V_{mem} is the total membrane volume. These useful relationships are extensively used to determine the void fraction and the axial dispersion coefficient of the porous medium.

3.1. External dispersion system

The system dispersion model contains two unknown variables, namely the PFR and the CSTR volumes, V_{PFR} and V_{CSTR}, respectively. The external system volume, V_{SYS}, may be properly measured from pulse experiments obtained in the absence of the membrane stack

Table 3
Determination of the model parameters used in the simulations.

Model	Parameters	Eq. no.	Evaluation source	Independent from dynamic chromatographic cycles
External system dispersion	V_{sys}	Eq. (46)	Moment analysis	Yes
	V_{CSTR}	Eqs. (13) and (14)	Best fit of system dispersion experiments	Yes
	V_{PFR}	Eq. (1)	External volume constraint	Yes
Membrane properties	ε	Eq. (47)	Mercury intrusion porosimetry; moment analysis	Yes
	α	Eq. (50)	Moment analysis	Yes
Column model				
Adsorption stage	q_m	Eq. (24)	Best fit of equilibrium binding data	Yes
	K_d	Eq. (24)	Best fit of equilibrium binding data	Yes
	k_a	Eq. (23)	Best fit of breakthrough curves[a]	No
Washing stage	–	–	–	–
Elution stage	k_e	Eqs. (32)and (33)	Best fit of elution peaks	No
	$c_{e,crit}$	Eqs. (32) and (33)	Best fit of elution peaks	No

[a] The adsorption kinetic rate constant is not a fitting parameter in the present work, and whenever binding equilibrium holds true.

by applying the first moment analysis [59,60]:

$$V_{SYS} = F\mu_1^{ext} \tag{46}$$

Thus, in view of Eq. (1) only one value, e.g. V_{CSTR}, is left to characterize completely the external dispersion system. Such a value can be obtained by best fitting Eqs. (13) and (14) to the concentration profiles of the probe species exiting the system after a step increment in the feed concentration. Therefore, both parameters characterizing the external system dispersion are obtained from separate independent measurements.

3.2. Static and dynamic properties of the porous medium

The properties of the porous membrane entering the model are the total porosity, ε, and the axial dispersion coefficient, D_L; both parameters can be obtained independently of the chromatographic cycle.

A number of different experimental methods are available for the evaluation of the void fraction of a porous medium [61]. In particular, it can be either measured directly through intrusion porosimetry experiments, or alternatively through the method of moments using Eq. (44):

$$\varepsilon = \frac{F}{V_{mem}}\mu_1^{mem} \tag{47}$$

In the present work the void fraction was measured by mercury intrusion porosimetry [62] and compared with the value obtained from the method of moments.

The dispersion coefficient is normally estimated through the moment analysis technique and, in the absence of direct measurements, can be calculated by empirical equations such as the Chung and Wen [63] or the Gunn [64] correlations. However, the latter relationships are specifically developed for columns packed with spherical beads, and equivalent studies are not yet available for porous membranes.

In passing, we note that some authors consider the value of D_L coincident with the molecular diffusion coefficient, D_m, [16,28,37], but that assumption is rather poor in general and suffers from a lack of theoretical basis; in fact, it has been shown that the two coefficients may differ by several orders of magnitude [61].

The axial dispersion coefficients, $D_{L,j}$, of each species j, are determined by applying the method of moments through Eqs. (44) and (45), and in general conditions they vary with the chemical species considered. However, for uniform porous media completely filled with a single fluid phase, when the superficial velocity is uniform and $Pe >> 1$, the axial dispersion coefficient reduces to [65]:

$$D_L = \alpha v \tag{48}$$

where α is a geometrical parameter independent of the molecular species usually indicated as dispersivity coefficient. Consistently, every solute in the mobile phase has the same value for the dispersion coefficient:

$$D_{L,i} = D_{L,e} = D_L \tag{49}$$

In view of Eqs. (45) and (48) one has:

$$\alpha = \frac{L}{2}\frac{\overline{\mu}_2^{mem}}{(\mu_1^{mem})^2} \tag{50}$$

Therefore, both parameters ε and D_L characterizing the porous medium are obtained from independent separate measurements.

3.3. Adsorption isotherm

The equilibrium adsorption isotherm given by Eq. (24) contains two parameters: the maximum binding capacity, q_m, and the equilibrium dissociation constant, K_d. Both parameters can be determined by best fitting of binding equilibrium data, which are obtained independently of the chromatographic separation process.

3.4. Kinetic parameters

The kinetic parameters entering the species mass balance equations of the model are: (i) the adsorption kinetic constant, k_a, entering the description of the adsorption cycle, Eq. (23), whenever the adsorption kinetics is not very fast; (ii) the elution kinetic constants, $k_{e,1}$ or $k_{e,2}$, appearing in the simulation of the elution step, Eq. (32) or (33), respectively.

Both adsorption and elution kinetic parameters are intrinsically associated to the chromatographic process and cannot be determined through independent experiments. They must be used as adjustable parameters to best fit the experimental data observed for the adsorption and the elution stages, respectively. In addition, consistently with their physical meaning, both k_a and $k_{e,1}$ or $k_{e,2}$ must be independent of feed concentration as well as of fluid velocity in the porous medium. That is indeed a very strong and important constraint which is crucial for model validation.

In any event, from the comparison with the experimental data obtained in the present work it is possible to conclude that in the loading step equilibrium conditions between mobile and solid phase are attained very rapidly so that binding equilibrium applies. Therefore, binding/unbinding reaction kinetics do not affect the actual profile of the breakthrough curves and consequently the adsorption rate constant is no longer an adjustable parameter required by the model.

Finally, the elution kinetic equations contain also the critical eluent concentration, $c_{e,crit}$, as model parameter. Since its direct

Table 4
Operating conditions of the experiments performed on the reference system [34,51].

Operating parameter	Conditions inspected
c_0 (mg/ml)	0.14; 0.24; 0.27; 0.48; 0.92; 1.05; 1.34; 1.47; 2.03; 2.15
v (cm/h)	29; 58; 145; 290
F (ml/min)	1; 2; 5; 10

measurement is in general not simple and it is highly affected by experimental errors, it has been considered as an additional adjustable parameter for the elution stage.

In summary, the model description of the adsorption step may contain one adjustable parameter, k_a, when the binding reaction is relatively slow, whose value is independent of feed concentration and flow rate, or no adjustable parameter when the adsorption rate is so fast that instantaneous equilibrium holds between liquid solution and chromatographic support. The latter case was observed for the experimental data used in model validation. The elution step contains two adjustable parameters, namely the kinetic constant, $k_{e,1}$ or $k_{e,2}$, and the critical eluent concentration, $c_{e,crit}$, whose values are both independent of feed flow rate.

The parameters entering the model proposed are listed in Table 3 together with the indication of the procedure used for their independent measurements.

4. Model validation

4.1. Experimental reference system

The experimental system considered to perform model validation is the purification of human IgG by using B14-TRZ-Epoxy2 affinity membranes. A layered stack of 5 membranes 2.5 cm in diameter was inserted into a low protein adsorption cartridge and connected to an FPLC Akta Purifier 100 (GE Heathcare, Milan, Italy). The affinity membranes were preliminarily tested by feeding pure IgG solutions under the different operating conditions reported in Table 4. The details of the experimental procedures and of the results obtained are reported in separate works [34,51].

In addition, affinity cycles were performed with a cell culture supernatant containing monoclonal human IgG_1 at a concentration of 0.12 mg/ml. The flow rates investigated are 1 and 5 ml/min, corresponding to interstitial velocities in the membranes of 29 and 145 cm/h, respectively. Several other impurities are contained in that sample, beyond the target protein IgG, as it can be observed from the SEC chromatogram reported in Fig. 2 obtained with a Prootema 300 column (PSS, Mainz, Germany) after calibration with Bio-Rad Gel Filtration Standards (Biorad, Milan, Italy). For simulation purposes the contaminants are conveniently lumped into four pseudo-components, labeled as PC-1 to PC-4, respectively, characterized by their retention times indicated in the inset of Fig. 2.

4.1.1. System dispersion curves

In order to determine the values of V_{PFR} and V_{CSTR} characterizing the external volumes, system dispersion experiments have been carried out in the absence of the membrane stack, using a 0.4% acetone solution in water. The system dispersion experiments were performed as a conventional chromatographic cycle: the tracer solution was fed during the adsorption and elution steps, while during washing pure water was fed to the apparatus. The results show that the system dispersion parameters, V_{PFR} and V_{CSTR}, do not depend on the specific chromatographic stage considered. In particular, the values of total system volume and of the PFR volume appeared to increase slightly as the flow rate increased, while the CSTR volume remained constant, as it is shown in Table 5 and in Fig. 3. That behavior, which may appear an unexpected inconsistency, is indeed an artifact due to the time needed by the AKTA system for valve switching, which may artificially lead to higher volumes at higher flow rates. That is evident from the linearity between the calculated PFR volume and the volume flow rate, shown in Fig. 3 ($R^2 = 0.992$), where the slope of 1.5 s corresponds to the time delay associated to valve switching. Accordingly, the effective value of V_{PFR} is represented by the intercept at zero flow rate, i.e. 1.75 ml, while the constant CSTR volume is 0.69 ml. Both values of V_{PFR} and V_{CSTR} do not depend on flow rate, indicating that under the operating conditions investigated the regions of the system characterized by plug flow and mixing are globally well defined. Finally, it is worth remarking that the total system volume is 2.44 ml, namely more than 6 times higher than the membrane column volume (0.38 ml, see Table 6). That further strengthens the critical need of considering external system dispersion in the modeling of membrane chromatographic processes, at least at laboratory scale.

Table 5
Volumes obtained for the system dispersion model.

F (ml/min)	v (cm/h)	V_{SYS} (ml)	V_{PFR} (ml)	V_{CSTR} (ml)
1	29	2.48 ± 0.06	1.77 ± 0.02	0.71 ± 0.04
2	58	2.49 ± 0.05	1.82 ± 0.02	0.67 ± 0.03
5	145	2.55 ± 0.03	1.87 ± 0.02	0.68 ± 0.01
10	290	2.72 ± 0.08	2.01 ± 0.10	0.71 ± 0.02

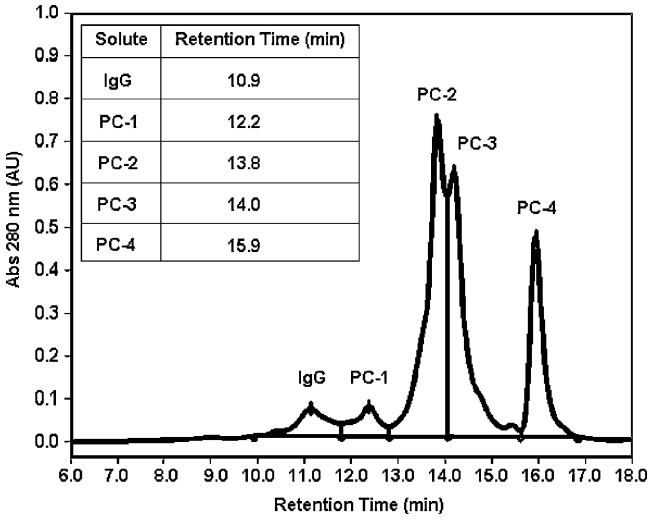

Fig. 2. Size exclusion chromatogram of the cell culture supernatant and retention times of the IgG and the pseudo-components representing the impurities present in the complex feed.

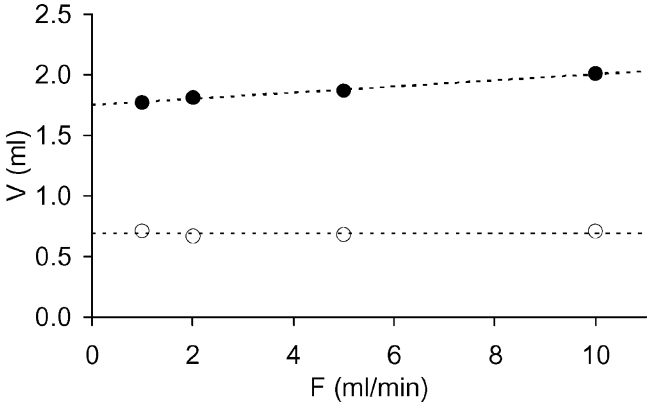

Fig. 3. Effect of the flow rate on the PFR (●) and CSTR (o) volumes obtained from the system dispersion model.

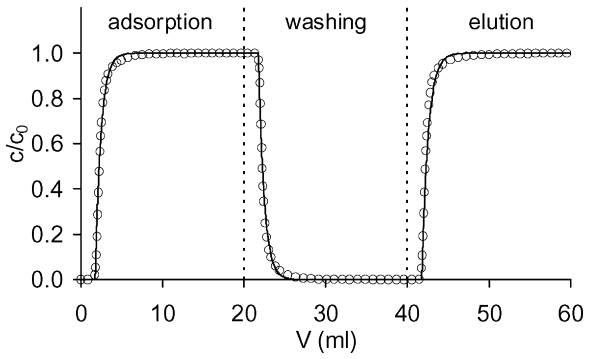

Fig. 4. Comparison between the experimental (o) and simulated (–) system dispersion curves for all the chromatographic stages. Interstitial flow velocity of 58 cm/h.

With the above values the typical comparison between simulation and dispersion experiments is reported in Fig. 4, showing the ability of the external dispersion model to describe the observed behavior during the whole cycle.

4.1.2. Affinity membrane properties

Pulse experiments were performed in the presence of the membrane stack using a 40% acetone solution as non-adsorbing tracer. The probe was injected from a 50 μl loop over a wide interval of interstitial velocities, ranging from 7 to 290 cm/h. Contributions from the extra column volumes were accounted for through system dispersion, as described in section 4.1.1.

The total porosity was estimated following two independent methods: the value resulting from the first moment analysis is 0.545 ± 0.068, while mercury intrusion porosimetry gave a value of 0.585 [62]. Since the two estimations are consistent and coherently with the fact that other membrane parameters were estimated through the moment analysis, model simulations were conducted using the former value.

The dispersivity coefficient in the membrane, α, was calculated from the first and the second moments using Eq. (50), obtaining a value of 0.104 ± 0.013 cm.

Although static equilibrium data are available in the literature for the system under investigation [51], their direct use was prudently not considered since important differences have been reported between equilibrium data determined by static and dynamic methods [29,66]. Therefore, binding equilibrium data in dynamic conditions were calculated by integration of the area behind the experimental loading curves up to 100% breakthrough, after the due correction for system dispersion effects [32]. The resulting data are reported in Fig. 5, and are properly described by the Langmuir adsorption isotherm shown by the continuous line.

The membrane physical properties and the Langmuir parameters obtained through independent measurements of dynamic binding capacity represent input data for the simulation model under study, and are summarized in Table 6.

Table 6
Geometrical constants and Langmuir parameters of the experimental reference system [34,51].

Variable	Value
L (cm)	0.10[a]
A (cm^2)	3.80
V_{mem} (ml)	0.38
ε	0.545
α (cm)	0.104
K_d (mg/ml)	0.037
$q_{m,100\%}$ (mg/ml)	6.97[b]

[a] Total length for a stack of 5 membranes.
[b] Value reported per unit solid volume.

4.2. Affinity cycles performed with pure IgG solutions

The model proposed to describe membrane affinity adsorbers has been detailed for all three affinity chromatographic steps, leading to a different set of PDE for each step. The relevant equations have been implemented in Aspen Custom Modeler simulation environment. The values of V_{PFR} and V_{CSTR} determined in Section 4.1.1 as well as the membrane properties reported in Section 4.1.2 are used as fixed input to the model.

The mathematical model is then used to simulate the experimental chromatographic cycles recorded at all feed concentrations and flow rates inspected. The choice of the solution strategy mostly depends on the chromatographic stage considered. In general, if adsorption cannot be considered infinitely fast, model simulations over the adsorption stage involve only one adjustable parameter, namely the adsorption kinetic rate constant, k_a. However, in the following it is demonstrated that for the system under investigation the protein–ligand interaction can be considered instantaneously at equilibrium, thus k_a is no longer an adjustable parameter and the model is fully predictive for the loading stage. For the washing step, in general, the model does not require any fitting parameter after system dispersion has been characterized and is thus used in a predictive mode also for this stage. Finally, for the simulation of the elution stage two fitting variables are present, namely the elution kinetic constant, $k_{e,1}$ or $k_{e,2}$, and the eluent critical concentration, $c_{e,crit}$.

The evaluation of the adjustable parameters has been carried out by applying the weighted least squares minimization method included in the software. It is worth noticing that parameter estimation was obtained by best fitting simultaneously the whole experimental data set at all feed flow rates and concentrations, and not considering separately the different flow rates or concentrations of the various affinity cycles performed. Hence, all the simulations use the same numerical values of the fitting parameters for all the operating condition considered. On the contrary, in order to obtain a seemingly superior fitting, many authors prefer to adjust the values of the fitting parameters for each specific operating condition adopted [18–22]. The latter procedure has two main drawbacks: first, the physical meaning of the adjustable parameters could vanish, as it is the case of the kinetic constant which are best fitted at very different values for different operating flow rates [18–22]; in addition, in this case the model cannot be considered fully validated and thus cannot be reliably used to extend the relevant conclusions under general conditions, as it is required for process optimization and scale up purposes.

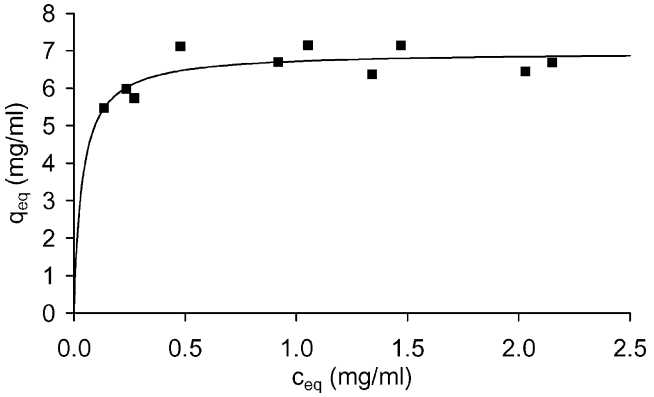

Fig. 5. Dynamic equilibrium binding data and Langmuir adsorption isotherm of human IgG onto B14-TRZ-Epoxy2 membranes.

4.2.1. Adsorption stage

In order to limit product loss and maximize productivity, in common practice the adsorption step is ended at the breakthrough point, when the effluent concentration reaches 10% of the feed value. Consequently, for industrial applications the onset of breakthrough is the most important portion of the entire breakthrough curve, which exploits only a small fraction of the theoretical adsorption capacity of the column. Nevertheless, in order to pursue a proper description of the actual breakthrough curve, with the possible exception of the behavior very close to complete column saturation at most, the conservative decision has been taken to describe the experimental curves as accurately as possible up to 80% breakthrough, thus considering a concentration range much larger than the one associated to the 10% breakthrough commonly considered in process practice.

The choice to focus the attention on the range up to 80% breakthrough for the simulation is motivated also by the fact that close to complete saturation, say above 80% BTC, the breakthrough curves usually show an approach to the final asymptotic value much slower than the one calculated by using any simple model kinetics able to follow the initial branch of the BTC curve, indicating that different behaviors come into play in protein adsorption as the final surface saturation is approached. The actual reasons for that behavior is not yet completely clear, even though it appears associated to protein–protein interactions at high surface coverage, where steric hindrance effects may be important [67–69], and possibly also to non-specific binding [29] or multilayer adsorption effects [70]. Disregarding what happens above 80% breakthrough implies also to consider in the simulations a reduced value of the maximum membrane capacity in order to be able to capture the actual lower portion of the breakthrough curve. In fact, we realize that use of the entire q_m value as input to the model would lead to a poor simulation not only of the final branch of the experimental curve, necessarily overestimated as already mentioned, but also of the initial branch, which correspondingly would be underestimated, due to the fact that the area above the breakthrough curve and below the system dispersion curve (see Fig. 6) measures the total dynamic binding capacity at 100% breakthrough. Therefore, in order to enable the model to simulate well the breakthrough curve up 80% BTC, neglecting the unspecified complex mechanism intervening above that value, we need to consider an effective reduced

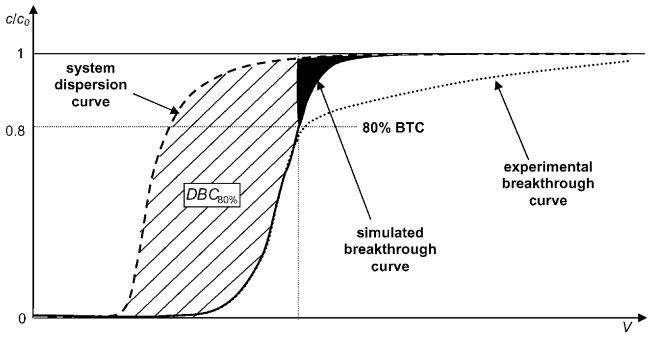

Fig. 6. Qualitative example of experimental and simulated breakthrough curves.

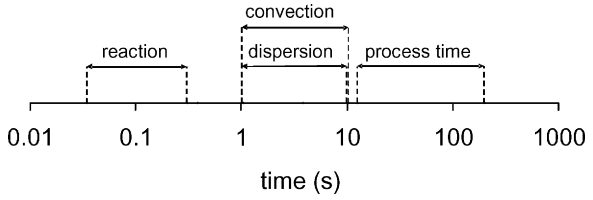

Fig. 7. Ranges of the reaction, convection, longitudinal dispersion and process characteristic times in Eqs. (28) for the system under investigation and under the operating conditions studied.

value of the maximum binding capacity, $q_{m,eff}$, not including the amount which is adsorbed through a different mechanism close to saturation. Such a reduced value is estimated in a simple way by inspecting the typical behavior shown in Fig. 6. It is apparent that the total amount of protein adsorbed in the solid phase associated to the breakthrough of the simulation model which describes well the experimental curve up to 80%, is given by two contributions: the first is the saturation reached up to 80% BTC, or $DBC_{80\%}$, indicated by the dashed area in Fig. 6; the second is the small amount indicated by the black area in Fig. 6. The latter is always smaller, or even much smaller, than 4% $DBC_{80\%}$ for all flow rates and feed concentrations investigated. Therefore, in general the effective maximum binding capacity, $q_{m,eff}$, is to all practical purposes the saturation reached at 80% breakthrough for the highest feed concentration, $c_{i,\infty}$, which lead to the maximum dynamic binding

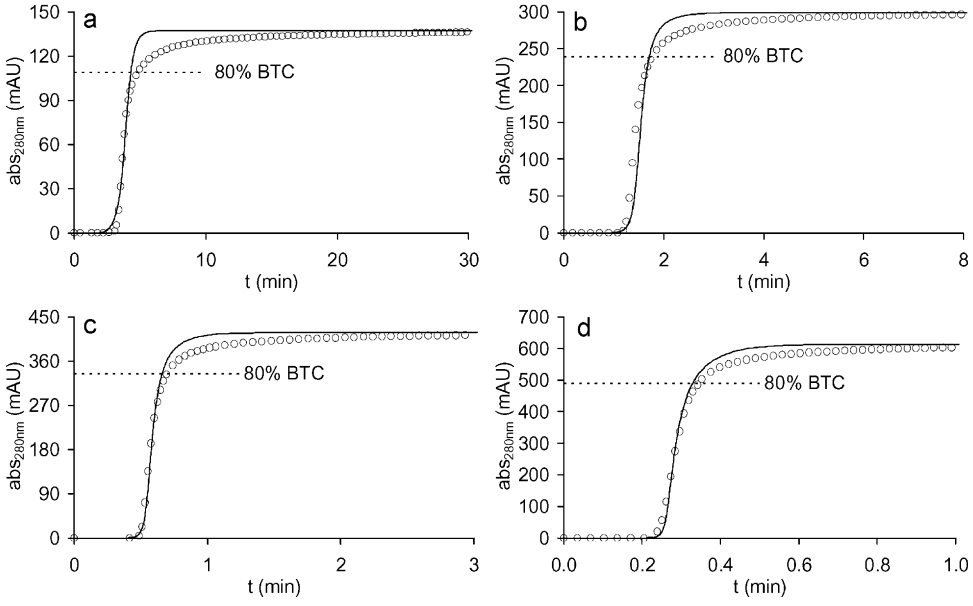

Fig. 8. Comparison between the experimental (o) and simulated (–) breakthrough curves at different operating conditions. (a) v = 29 cm/h, c_0 = 0.48 mg/ml; (b) v = 58 cm/h, c_0 = 1.05 mg/ml; (c) v = 145 cm/h, c_0 = 1.47 mg/ml; (d) v = 290 cm/h, c_0 = 2.15 mg/ml.

capacity:

$$q_{m,eff} = DBC_{80\%}|_{c_i=c_{i,\infty}} \quad (51)$$

That value is thus the effective maximum binding capacity to use as input to the model, in order to make the simulation potentially able to offer a good representation of the breakthrough curve up to 80%.

From the experimental BTC curves observed for the membranes used in the present work for all concentrations we obtain that $DBC_{80\%} = 0.627 DBC_{100\%}$; the corresponding saturation value of 62.7% is consistent with the results obtained by Montesinos-Cisneros et al. who report saturation values at 80% BTC in range between 0.38 and 0.71 [28].

After determining the effective binding capacity, the validity of the conditions reported in Eqs. (28) must be checked in order to determine whether the binding reaction is or not at equilibrium in the adsorption step. To that aim, the kinetic rate constant was first estimated by fitting the dynamic experiments using the non-equilibrium model, Eq. (23), considering Langmuir reversible kinetics. The best fitted value for the adsorption kinetic rate constant, k_a, was equal to 808.3 ± 59.3 ml/(mg min). The comparison between the characteristic time scales presented in Eqs. (28) for the system under investigation, with the operating conditions adopted, is reported in Fig. 7.

For every flow rate and feed concentration investigated, the reaction time scale is much smaller than both the process time and the characteristic time scales for convection and longitudinal dispersion. Therefore, reaction kinetics is much faster than the other main transport mechanisms, so that equilibrium may be considered for the adsorption reaction.

In addition, the time scale for convection, τ_C, ranges between 1.2 and 12.4 s, while the characteristic time for axial dispersion, τ_L, varies between 1.2 and 11.9 s. The two phenomena have characteristic times of the same order of magnitude, confirming that axial dispersion is one of the major transport mechanisms occurring in membrane adsorbers.

Consequently, the equilibrium dispersive model, Eq. (26), was applied to generate the simulations of the breakthrough curve for the system studied. In the absence of adjustable parameters the simulations are completely predictive and their typical comparison with experimental results is presented by the examples reported in Fig. 8.

The simulations of the adsorption step are in apparent good agreement with the experimental results up to 80% breakthrough. Remarkably, the dispersive equilibrium model is able to properly describe the slope at the onset of breakthrough; on the contrary, should system dispersion effects be neglected, the resulting breakthrough curve would show a sudden steep increase in the outlet concentration in correspondence of column saturation [71]. It is possible to conclude that breakthrough broadening in the initial front of the adsorption curve is accounted for well by the dispersive term at all flow rates and concentrations considered.

Near membrane saturation, significant broadening occurs and, as already discussed, the model prediction deviates from the experimental curve, with deviations depending on the operating condition.

4.2.2. Washing stage

No adjustable parameters are present in the simulations of the washing curves. Typical model calculations obtained under different operating conditions are reported in Fig. 9, together with the experimental data collected.

Clearly, the simulations describe rather well the experimental data in almost the entire washing curve, capturing properly the fast concentration decline; however, the experimental concentration tails at longer times are slightly underestimated by the simulations, starting at solute concentration lower than approximately 0.14 mg/ml, equivalent to an absorbance signal around 40 mAU.

The washing step is conservatively carried out by feeding 50 column volumes of washing buffer, much more than the 10 column volumes usually recommended in affinity purifications [72]. At the end of the washing step the experimental curves reach the UV baseline indicating that no protein is further released. The amount of protein washed out during this stage, averaged over all the chromatographic runs performed, is equal to 23.7% of the protein totally adsorbed during breakthrough, while the residual 76.3% still remains bound onto the membranes and cannot be washed out but only subsequently eluted.

4.2.3. Elution stage

Very little work on the simulation of the elution step in affinity chromatography is available in the literature, and only a few papers consider membrane adsorbers devices [19,22]. In the latter works, however, the values of the fitting parameters are adjusted for every operating condition investigated, obtaining in particular different values of the kinetic constants at different flow rates; hence it is very difficult to believe that model validation in the elution step was achieved.

The main mathematical difference between the description of adsorption and elution is represented by surface reaction kinetics. To a first order approximation, it is plausible that the elution mechanism involves irreversible kinetics given by Eq. (32) or (33), which contain two parameters given by the elution kinetic rate constant, $k_{e,1}$ or $k_{e,2}$, and by the critical eluent concentration, $c_{e,crit}$. Clearly both factors cannot be determined from independent measurements and must be considered as fitting parameters.

In particular, since desorption is very sensitive to pH changes, the effective eluent has been considered as H^+, so that the critical eluent concentration, $c_{e,crit}$, was equivalently reported in terms of critical pH value as:

$$pH_{crit} = -\log[H^+]_{crit} = -\log[c_{e,crit}] \quad (52)$$

The critical pH represents the second fitting parameter for the elution stage.

Some relevant experiments are compared in Fig. 10 with simulation results generated using the two proposed kinetic equations, Eqs. (32) and (33). The values of the two adjustable parameters were obtained by best fitting the model calculations to all the experimental elution curves obtained at all feed flow rates and concentrations inspected; the resulting values are listed in Table 7.

The shape of the experimental elution peaks vary with eluent flow rate, and in particular their height decreases with increasing flow rate, while the total amount of protein recovered is not affected by linear velocity [34,51]. Simulations are able to describe the same trend, although they do not fit the experimental results as well as they did for the adsorption and washing stages. In particular, at the higher flow rate investigated the simulated peak is taller and narrower than the experimental result; vice versa, at the lower superficial velocity the model leads to a peak lower and wider with respect to the observed one. That trend is more pronounced for the pseudo first order elution kinetics, which is more influenced by flow rate changes, while the second order elution kinetics is affected to a minor extent. That is reflected by the time scale for elution calculated from the best-fitted values of the elution kinetic rate constant: for the second order elution kinetics one has $\tau_e = 1/(k_{e,2} \cdot c_e) = 2.03$ s, while $\tau_e = 1/k_{e,1} = 5.71$ s for the pseudo first order elution kinetics. In both cases, however, the characteristic time of desorption is comparable to those of convection and axial dispersion, which justifies the significant variation of the elution peaks with flow rate.

An additional difference between the simulations generated using the two kinetic equations can be observed at the onset of the elution peaks, where dispersion effects are present and the eluent

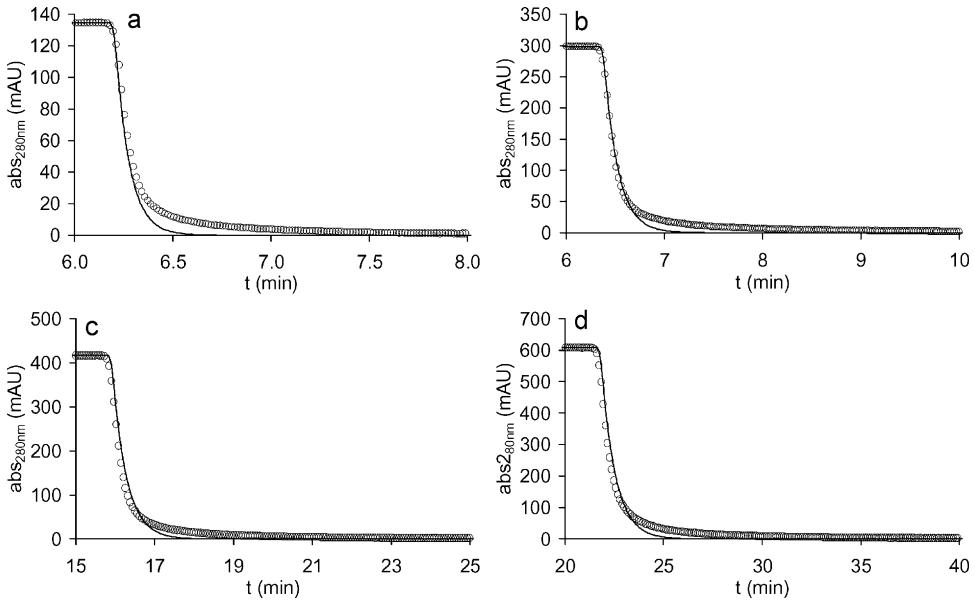

Fig. 9. Comparison between the experimental (o) and simulated (–) washing curves at different operating conditions. (a) $v = 290$ cm/h, $c_0 = 0.48$ mg/ml; (b) $v = 145$ cm/h, $c_0 = 1.05$ mg/ml; (c) $v = 58$ cm/h, $c_0 = 1.47$ mg/ml; (d) $v = 29$ cm/h, $c_0 = 2.15$ mg/ml.

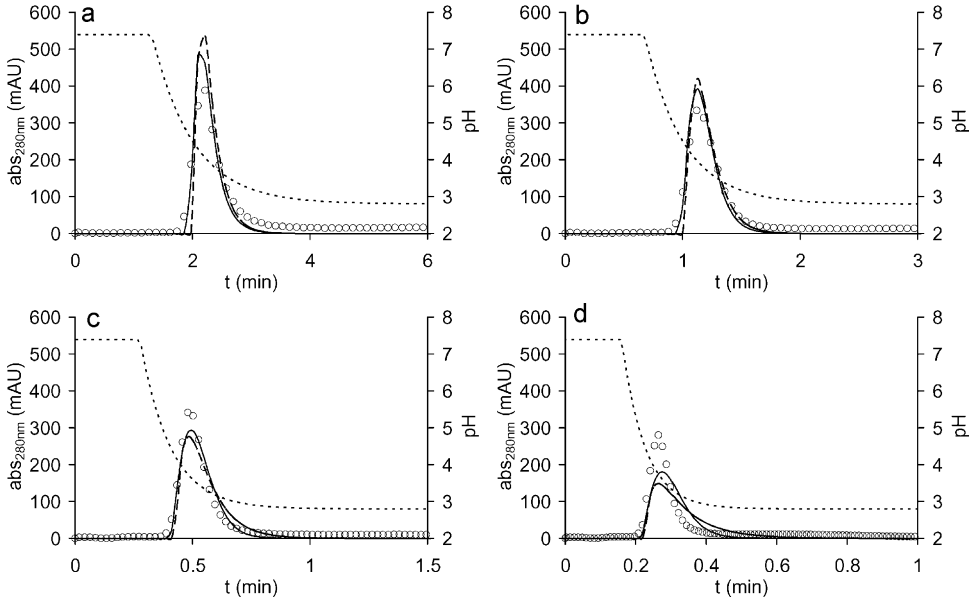

Fig. 10. Comparison between experimental (o) and simulated elution curves at different operating conditions. Solid lines: second order elution kinetics; dashed lines: pseudo first order elution kinetics; dotted lines: pH profile. (a) $v = 29$ cm/h, $c_0 = 0.48$ mg/ml; (b) $v = 58$ cm/h, $c_0 = 1.05$ mg/ml; (c) $v = 145$ cm/h, $c_0 = 1.47$ mg/ml; (d) $v = 290$ cm/h, $c_0 = 2.15$ mg/ml.

concentration is still increasing towards its feed value. Using the second order kinetic equation the elution rate is initially smaller and then increases as the eluent concentration increases, leading to peaks smoother than those calculated by the pseudo first order kinetics, which, on the contrary, gives sharper front peaks due to a faster protein desorption rate, at the critical pH, independent of the eluent concentration. The second order kinetic equation is clearly more satisfactory to describe elution.

Finally, the introduction of the critical pH in the elution mechanism is capable to return model simulations that approximate well the starting point of the experimental peaks. The main effect produced by the presence of a critical eluent concentration is to properly delay in time the simulated peaks, which instead would start much earlier if the elution onset would begin as soon as the eluent contacts the membrane surface.

Table 7
Best fitted values of the adjustable parameters in the elution stage.

Elution kinetic equation	k_e	pH_{crit}
Second order reaction, Eq. (32)	$(93.48 \pm 2.52) \times 10^3$ ml/(mg min)	4.8 ± 0.2
Pseudo first order reaction, Eq. (33)	10.51 ± 0.20 1/min	4.7 ± 0.2

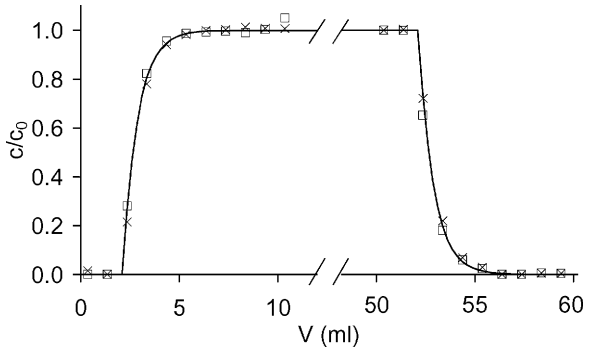

Fig. 11. Comparison between the experimental breakthrough and washing curves for the two main pseudo-components and the system dispersion model. Linear velocity of 145 cm/h. PC-1 (□), PC-2 (x), simulation (–).

4.3. Affinity cycles performed with the cell culture supernatant

In the case of chromatographic cycles performed with cell culture supernatant one needs to describe separately the behavior of the different impurities and that of the monoclonal IgG present. The four pseudo-components, which globally represent the impurities, do not interact directly with the ligand which is specific for IgG, and therefore they are considered as inert species, whose breakthrough and washing curves can be calculated in an entirely predictive way using the system dispersion model only, with the same values of model parameters already determined.

The experimental breakthrough and washing curves for the two major pseudo-components are reported in Fig. 11 together with the simulation results. The ability of the system dispersion model to predict the experimental data is outstanding. This important result is a clear indication of the absence of interactions between the impurities contained in the complex feed and the B14 ligand immobilized on the membranes investigated.

Based on that, the interactions between ligand and IgG are expected to be unaffected by the impurities present in the complex mixture. Accordingly, the adsorption behavior of IgG has been simulated by using the column model coupled with the system dispersion model as it has been done for pure IgG solutions, using the same values of the model parameters which were obtained for pure IgG solutions. It is possible to remark that the breakthrough curves for IgG broaden close to the saturation conditions, similarly to what already observed for the adsorption curves of pure IgG solutions.

Two comparisons between experimental measurements and simulation results are presented in Fig. 12 for two different operating conditions. The excellent agreement that is apparent up to 80% breakthrough clearly demonstrates the robustness and predictive ability of the model, as well as the reliability of the assumptions made. In parallel, such results also indicate the high specificity of the immobilized ligand towards the IgG species, which allow to calculate the chromatographic behavior of complex mixtures simply on the basis of the parameters obtained for pure IgG solutions.

Unfortunately, as a consequence of the limits of the fraction collector in the AKTA instrumentation, the frequency of collected fractions in the elution stage was not sufficient to guarantee a detailed description of the experimental elution peak, as it is required for a proper comparison between simulation and experiments. However, in the adsorption and washing steps the behavior of IgG contained in the complex feed could be reliably predicted by the model previously calibrated with experiments carried out by feeding pure IgG solutions. Therefore it is very reasonable to expect that also during elution the proposed model will hold with the same values for the kinetic constant and critical pH resulting from the simulations of pure IgG tests, since the elution stage contains a much smaller amount of impurities than the adsorption and washing stages.

5. Conclusions

A mathematical model for the description of protein purification through membrane affinity chromatography has been studied. The model considers all the steps of a complete chromatographic cycle: adsorption, washing and elution, as well as the external system dispersion, and leads to predictive simulations for adsorption up to 80% BTC and for washing, at all concentrations and flow rates.

Time scale analysis indicated that boundary layer mass transfer can always be disregarded with respect to axial convection and longitudinal dispersion in the membrane.

The model is physically based; all its parameters have a precise physical meaning and their values can generally be obtained through independent measurements of dynamic binding capacity, different from the chromatographic process; this feature confers solidity and predictive ability to the model. Only the parameters that are intrinsically associated to the adsorption/elution kinetics are considered as adjustable parameters and are best fitted to the experimental chromatographic data; in all cases they are independent of fluid flow rate, according to their physical meaning.

The reference system used to validate the model is the separation of human IgG from a cell culture supernatant by using B14-TRZ-Epoxy2 affinity membranes. In order to check the effectiveness of the proposed model, a broad data set of affinity cycles performed with pure IgG solutions were initially considered to test the model and to determine the kinetic parameters of adsorption and elution. The results of the simulation model describe very well the experimental data and show reliability in several aspects; in particular:

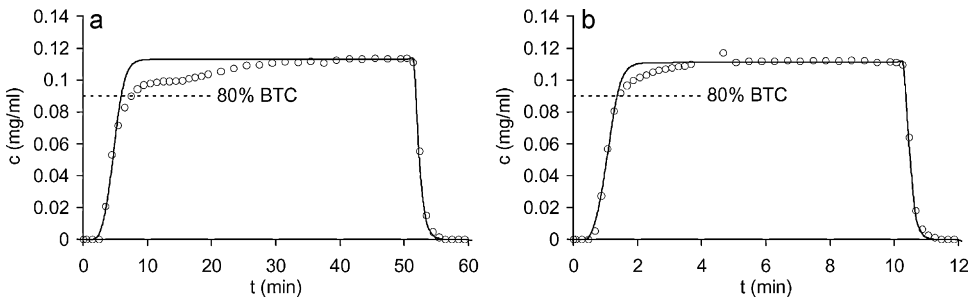

Fig. 12. Comparison between the experimental (o) and simulated (–) breakthrough and washing curves for the IgG species in the runs performed with the complex feedstock at two different linear velocities. (a) $v = 29$ cm/h and (b) $v = 145$ cm/h.

(i) the independence of the breakthrough curves from flow rate is well explained by the equilibrium binding reaction between IgG and the immobilized ligand, which appears to be a general feature for membrane chromatographic systems;
(ii) the slope of the adsorption and washing curves is well described by the dispersive term of the mass balance equation, which is a crucial contribution to describe the behavior of membrane adsorbers;
(iii) model simulations over the elution stage are able to represent the general trend of the experimental elution peaks, especially with regard to their flow rate dependence, indicating that elution rate has the same order of magnitude of the other mass transport mechanisms, and is described by an irreversible kinetic equation.

Application of the model to describe the experiments performed with cell culture supernatant is entirely predictive, based on the kinetic parameters obtained for pure IgG solutions. The simulations are in excellent agreement with the experimental data both for the impurities and for the IgG species, without the need of any additional fitting parameter.

The proposed model is thus fully validated for the system investigated, and can be considered a reliable tool also for other experimental systems and other affinity membrane chromatography devices, either for process design or for optimization and scale up purposes.

Acknowledgements

This work has been performed as part of the "Advanced Interactive Materials by Design" (AIMs) project, supported by the Sixth Research Framework Programme of the European Union (NMP3-CT-2004-500160).

References

[1] L.S. Lerman, Proc. Natl. Acad. Sci. 39 (1953) 232.
[2] A.I. Liapis, J. Biotechnol. 11 (1989) 143.
[3] K. Huse, H.J. Böhme, G.H. Scholz, J. Biochem. Biophys. Methods 51 (2002) 217.
[4] D. Low, R. O'Leary, N.S. Pujar, J. Chromatogr. B 848 (2007) 48.
[5] E. Klein, Affinity Membranes: Their Chemistry and Performance in Adsorptive Separation Processes, Wiley, New York, 1991.
[6] X.F. Zeng, E. Ruckenstein, Biotechnol. Prog. 15 (1999) 1003.
[7] E. Klein, J. Membr. Sci. 179 (2000) 1.
[8] H. Zou, Q. Luo, D. Zhou, J. Biochem. Biophys. Methods 49 (2001) 199.
[9] R. Ghosh, J. Chromatogr. A 952 (2002) 13.
[10] F.H. Arnold, H.W. Blanch, C.R. Wilke, Chem. Eng. J. 30 (1985) B9.
[11] A. Tejeda-Mansir, R.M. Montesinos, R. Guzmán, J. Biochem. Biophys. Methods 49 (2001) 1.
[12] G. Guiochon, J. Chromatogr. A 965 (2002) 129.
[13] K. Kaczmarski, A. Cavazzini, P. Szabelski, D. Zhou, X. Liu, G. Guiochon, J. Chromatogr. A 962 (2002) 57.
[14] G. Wang, R.G. Carbonell, J. Chromatogr. A 1078 (2005) 98.
[15] H.O. Herigstad, P.V. Gurgel, R.G. Carbonell, Biotechnol. Prog. (2010), doi:10.1002/btpr.502.
[16] K. Miyabe, G. Guiochon, J. Chromatogr. A 890 (2000) 211.
[17] G. Guiochon, A. Felinger, D.G. Shirazi, A.M. Katti, Fundamentals of Preparative and Nonlinear Chromatography, 2nd ed., Elsevier, San Diego, 2006.
[18] J.R. Sportsman, G.S. Wilson, Anal. Chem. 52 (1980) 2013.
[19] W. Hao, J. Wang, X. Zhang, J. Chromatogr. A 1114 (2006) 123.
[20] A. Puerta, C. Vidal-Madjar, A. Jaulmes, J.C. Diez-Masa, M. de Frutos, J. Chromatogr. A 1119 (2006) 34.
[21] H. Bak, O.R.T. Thomas, J. Abildskov, J. Chromatogr. B 848 (2007) 131.
[22] P. van Beijeren, P. Kreis, A. Hoffmann, M. Mutter, S. Sommerfeld, W. Bäcker, A. Górak, Chem. Pap. 62 (2008) 458.
[23] D. Cecchini, J. Ganguli, J. Pieracci, J. Thommes, Modeling of Industrial Scale Purification Processes Using Multivariate Analysis and Principal Component Analysis, in: Recovery of Biological Products XIV Conference, Lake Tahoe, CA, 2010.
[24] S.Y. Suen, M.R. Etzel, Chem. Eng. Sci. 47 (1992) 1355.
[25] H.C. Liu, J.R. Fried, AIChE J. 40 (1994) 40.
[26] K.H. Gebauer, J. Thömmes, M.R. Kula, Chem. Eng. Sci. 52 (1997) 405.
[27] W. Hao, J. Wang, Chromatographia 62 (2005) 55.
[28] R.M. Montesinos-Cisneros, J. de la Vega Olivas, J. Ortega, R. Guzmán, A. Tejeda-Mansir, Biotechnol. Prog. 23 (2007) 881.
[29] C. Boi, S. Dimartino, G.C. Sarti, J. Chromatogr. A 1162 (2007) 24.
[30] F.T. Sarfert, M.R. Etzel, J. Chromatogr. A 764 (1997) 3.
[31] R. Hahn, A. Tscheliessnig, P. Bauerhansl, A. Jungbauer, J. Biochem. Biophys. Methods 70 (2007) 87.
[32] S.E. Bower, S.R. Wickramasinghe, J. Membr. Sci. 330 (2009) 379.
[33] F. Morselli, Graduate Thesis, Università di Bologna, Bologna, 2008.
[34] S. Dimartino, Ph.D. Thesis, Università di Bologna, Bologna, 2009.
[35] A.M. Athalye, S.J. Gibbs, E.N. Lightfoot, J. Chromatogr. 384 (1987) 285.
[36] D.K. Roper, E.N. Lightfoot, J. Chromatogr. A 702 (1995) 69.
[37] S.Y. Suen, M.R. Etzel, J. Chromatogr. A 686 (1994) 179.
[38] R.B. Bird, W.E. Stewart, E.N. Lightfoot, Transport Phenomena, 2nd ed., Wiley, New York, 2002.
[39] K.G. Briefs, M.R. Kula, Chem. Eng. Sci. 47 (1992) 141.
[40] J.E. Kochan, Y.J. Wu, M.R. Etzel, Ind. Eng. Chem. Res. 35 (1996) 1150.
[41] O.P. Dancette, J.L. Taboureau, E. Tournier, C. Charcosset, P. Blond, J. Chromatogr. B 723 (1999) 61.
[42] H.N. Endres, J.A.C. Johnson, C.A. Ross, J.K. Welp, M.R. Etzel, Biotechnol. Appl. Biochem. 37 (2003) 259.
[43] C. Boi, S. Dimartino, G.C. Sarti, Biotechnol. Prog. 24 (2008) 640.
[44] J. Wang, F. Dismer, J. Hubbuch, M. Ulbricht, J. Membr. Sci. 320 (2008) 456.
[45] M.T. Tyn, T.W. Gusek, Biotechnol. Bioeng. 35 (1990) 327.
[46] J.A. Gerstner, R. Hamilton, S.M. Cramer, J. Chromatogr. 596 (1992) 173.
[47] D.D. Frey, R. Van de Water, B. Zhang, J. Chromatogr. 603 (1992) 43.
[48] A. Shiosaki, M. Goto, T. Hirose, J. Chromatogr. A 679 (1994) 1.
[49] P.V. Danckwerts, Chem. Eng. Sci. 2 (1953) 1.
[50] I. Langmuir, J. Am. Chem. Soc. 38 (1916) 2221.
[51] C. Boi, S. Dimartino, S. Hofer, J. Horak, S. Williams, W. Lindner, G.C. Sarti, Influence of different spacer arms on A2P and B14 affinity membranes for human IgG purification, J. Chromatogr. B (submitted for publication).
[52] B.H. Arve, A.I. Liapis, Biotechnol. Bioeng. 31 (1988) 240.
[53] H.A. Chase, Chem. Eng. Sci. 39 (1984) 1099.
[54] M. Kubin, Collect. Czech. Chem. Commun. 30 (1965) 2900.
[55] E. Kučera, J. Chromatogr. 19 (1965) 237.
[56] J.C. Sternberg, Adv. Chromatogr. 2 (1966) 205.
[57] L. Hong, A. Felinger, K. Kaczmarski, G. Guiochon, Chem. Eng. Sci. 59 (2004) 3399.
[58] F.H. Arnold, H.W. Blanch, C.R. Wilke, Chem. Eng. J. 30 (1985) B25.
[59] D.B. Spalding, Chem. Eng. Sci. 9 (1958) 74.
[60] E.N. Lightfoot, A.M. Lenhoff, R.L. Rodriguez, Chem. Eng. Sci. 37 (1982) 954.
[61] F.A.L. Dullien, Porous Media: Fluid Transport and Pore Structure, 2nd ed., Academic Press, San Diego, 1992.
[62] C. Boi, S. Dimartino, M. Giovannangelo, G.C. Sarti, E. van de Ven, L. Versteeg Bolhuis, Z. Borneman, Correlation of material structure and performance for affinity membranes, Deliverable no. 5.14, internal report of Integrated EU Project AIMs, 2008.
[63] S.F. Chung, C.Y. Wen, AIChE J. 14 (1968) 857.
[64] D.J. Gunn, Chem. Eng. Sci. 42 (1987) 363.
[65] J. Baer, Y. Bachmat, Introduction to Modeling of Transport Phenomena in Porous Media, Kluwer Acad. Publ., Derdrecht, 1990 (Chapter 6).
[66] H. Yang, C. Viera, J. Fischer, M.R. Etzel, Ind. Eng. Chem. Res. 41 (2002) 1597.
[67] A. Jungbauer, Curr. Opin. Biotechnol. 7 (1996) 210.
[68] X. Jin, J. Talbot, N.H.L. Wang, AIChE J. 40 (1994) 1685.
[69] J. Talbot, G. Tarjus, P.R. Van Tassel, P. Viot, Colloids Surf. A 165 (2000) 287.
[70] L.R. Castilho, F.B. Anspach, W.D. Deckwer, J. Membr. Sci. 207 (2002) 253.
[71] A. Seidel-Morgenstein, J. Chromatogr. A 1037 (2004) 255.
[72] J.M. Walker, The Protein Protocols Handbook, 2nd ed., Humana Press, Totowa, 2002.